Open access • Journal Article • DOI:10.1021/ACSAMI.5B06801

Low-temperature plasma-assisted atomic layer deposition of silicon nitride moisture permeation barrier layers — Source link

Anne-Marije Andringa, Alberto Perrotta, Koen de Peuter, Harm C. M. Knoops ...+3 more authors

Institutions: Eindhoven University of Technology, Oxford Instruments

Published on: 30 Sep 2015 - ACS Applied Materials & Interfaces (American Chemical Society)

Topics: Atomic layer deposition, X-ray photoelectron spectroscopy and Silicon nitride

Low-temperature plasma-assisted atomic layer deposition of silicon nitride moisture permeation barrier layers

ACS APPLIED MATERIALS & INTERFACES

Research Article

www.acsami.org

Low-Temperature Plasma-Assisted Atomic Layer Deposition of Silicon Nitride Moisture Permeation Barrier Layers

Anne-Marije Andringa,[†] Alberto Perrotta,[†,‡] Koen de Peuter,[†] Harm C. M. Knoops,[†,§] Wilhelmus M. M. Kessels,[†,∥] and Mariadriana Creatore*[,†,∥]

[†]Department of Applied Physics, Eindhoven University of Technology, P.O. Box 513, 5600 MB Eindhoven, The Netherlands

[‡]Dutch Polymer Institute (DPI), P.O. Box 902, 5600 AX Eindhoven, The Netherlands

[§]Oxford Instruments Plasma Technology, North End, Bristol BS49 4AP, United Kingdom

[∥]Solliance Solar Research, High Tech Campus 5, 5656 AE Eindhoven, The Netherlands

ABSTRACT: Encapsulation of organic (opto-)electronic devices, such as organic light-emitting diodes (OLEDs), photovoltaic cells, and field-effect transistors, is required to minimize device degradation induced by moisture and oxygen ingress. SiN_x moisture permeation barriers have been fabricated using a very recently developed low-temperature plasma-assisted atomic layer deposition (ALD) approach, consisting of half-reactions of the substrate with the precursor $SiH_2(NH^tBu)_2$ and with N_2-fed plasma. The deposited films have been characterized in terms of their refractive index and chemical composition by spectroscopic ellipsometry (SE), X-ray photoelectron spectroscopy (XPS), and Fourier-transform infrared spectroscopy (FTIR). The SiN_x thin-film refractive index ranges from 1.80 to 1.90 for films deposited at 80 °C up to 200 °C, respectively, and the C, O, and H impurity levels decrease when the deposition temperature increases. The relative open porosity content of the layers has been studied by means of multisolvent ellipsometric porosimetry (EP), adopting three solvents with different kinetic diameters: water (~0.3 nm), ethanol (~0.4 nm), and toluene (~0.6 nm). Irrespective of the deposition temperature, and hence the impurity content in the SiN_x films, no uptake of any adsorptive has been observed, pointing to the absence of open pores larger than 0.3 nm in diameter. Instead, multilayer development has been observed, leading to type II isotherms that, according to the IUPAC classification, are characteristic of nonporous layers. The calcium test has been performed in a climate chamber at 20 °C and 50% relative humidity to determine the intrinsic water vapor transmission rate (WVTR) of SiN_x barriers deposited at 120 °C. Intrinsic WVTR values in the range of 10^{-6} g/m^2/day indicate excellent barrier properties for ALD SiN_x layers as thin as 10 nm, competing with that of state-of-the-art plasma-enhanced chemical vapor-deposited SiN_x layers of a few hundred nanometers in thickness.

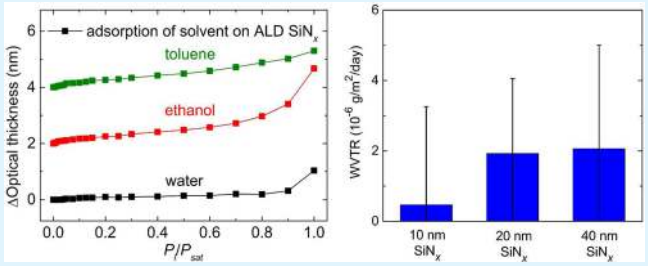

KEYWORDS: *atomic layer deposition, plasma, silicon nitride, moisture permeation barrier layers, ellipsometric porosimetry, calcium test*

1. INTRODUCTION

Emerging technologies such as organic light-emitting diode lighting and displays, organic thin-film transistors, and thin-film solar cells have become very attractive due to their performance in combination with their mechanical flexibility and large-area processing compatibility.[1] However, in order for these devices to have a long lifetime and high reliability, there are a number of challenges to be overcome. One of them is the efficient encapsulation of the device against moisture and oxygen permeation, which otherwise severely affects the working device, as has been extensively shown in the case of OLEDs[2,3] or thin-film organic solar cells.[4,5] To ensure a lifetime of 10 years for OLEDs, an encapsulation layer is required with a water vapor transmission rate (WVTR) of 10^{-6} g/m^2/day. For moisture permeation barrier layers on flexible devices, developed on polymer substrates, there is also need for large-area, low-temperature processing.

Barrier layer solutions commonly adopt inorganic thin films deposited by sputtering, plasma-enhanced chemical vapor deposition (PECVD), and (plasma-assisted) atomic layer deposition (ALD).[6−9] Recently, ALD has been acknowledged as the deposition method of choice to yield high-quality, densely packed, conformal, nearly pinhole-free inorganic layers due to its sequential, self-limiting nature.[10−18] For example, Carcia et al. measured an effective WVTR for 25 nm thick Al_2O_3 films of 1.7×10^{-5} g/m^2/day at 38 °C and 85% relative humidity (RH).[11] Also, Graham et al. report an effective WVTR of 2.0×10^{-5} g/m^2/day for a hybrid layer consisting of SiO_x or SiN_x fabricated by PECVD and Al_2O_3 added by ALD.[19] Yong-Qiang et al. reported an effective WVTR of 8.7×10^{-6} g/

Received: July 26, 2015
Accepted: September 22, 2015
Published: September 22, 2015

DOI: 10.1021/acsami.5b06801
ACS Appl. Mater. Interfaces 2015, 7, 22525−22532

m^2/day for Al_2O_3 deposited by ALD with O_3 at 80 °C for 81 nm thick films.[12] Seo et al. tested water permeation through 60 nm thick ALD TiO_2 barriers and found an effective WVTR of 6×10^{-4} g/m^2/day.[14] Generally, it can be concluded that thinner ALD layers are found to outperform thicker PECVD or sputtered layers in terms of barrier performance.

Water permeation has been universally found to occur unhindered through local pinholes/defects present in the inorganic layer.[20,21] Therefore, a more effective approach to water barrier performance consists of developing multilayers of inorganic barrier layers and polymer-like interlayers, the latter of which have been shown to provide a defect decoupling effect, thereby reducing the number of substrate-induced pinholes in the subsequent barrier layer. Such an approach can lead to barriers 3 orders of magnitude less permeable to water and oxygen than that of a single inorganic layer.[22−25]

Next to local defects, water permeation occurs also through the (bulk) nanoporosity of the inorganic barrier.[26,27] Previously, we have reported on the correlation among the intrinsic barrier properties, pore size, and relative pore content of PECVD and plasma-assisted ALD inorganic (e.g., SiO_2 and Al_2O_3) barriers. [The "intrinsic" barrier properties are responsible for the water permeation through the bulk of the barrier, whereas the total water permeation, including the local water permeation through pinholes/defects, defines the "effective" barrier properties.] Pores larger than 1 nm with a relative content above 1% have been found to be responsible for mediocre barrier layers characterized by a WVTR in the range of 10^{-2} to 10^{-3} g/m^2/day, whereas pore sizes in the range between 0.3 and 1 nm have been found to be responsible for the transition from medium (10^{-4} g/m^2/day) to excellent (10^{-6} g/m^2/day) intrinsic barrier performance.[28,29] Therefore, it is essential to control not only the local defect density but also the nanoporosity of the inorganic layer. In this respect, Keuning et al. reported a 20 nm thick plasma assisted-ALD Al_2O_3 film with an excellent intrinsic WVTR of 2×10^{-6} g/m^2/day.[10] For comparison, an intrinsic WVTR for PECVD SiN_x on the same order of magnitude has been reported for thickness values above 170 nm.[10,30]

In this work, we investigated the moisture permeation barrier properties of plasma-assisted ALD SiN_x layers. Deposition of high-quality SiN_x by ALD is very challenging in terms of controlling the impurity levels in the layer, especially when operating at substrate temperatures (T_{sub}) compatible with thermally sensitive substrates.[31,32] Using a plasma-assisted ALD process recently developed in our group, SiN_x can be prepared at a temperature between 80 and 200 °C by alternating bis(tertiary-butylamino)silane ($SiH_2(NH^tBu)_2$, BTBAS) precursor dosing and N_2 plasma exposure.[33,34] This halogen-free process yields SiN_x films over a wide temperature range, yielding close to stoichiometric Si_3N_4 films for high temperatures (400−500 °C). At lower temperatures, the films contain carbon and hydrogen originating from the organic precursor. The impurity content can be reduced by applying long plasma exposure, low plasma pressures, and/or high substrate temperatures.

The ALD SiN_x barrier films were optically and chemically characterized by means of spectroscopic ellipsometry (SE), X-ray photoelectron spectroscopy (XPS), and Fourier-transform infrared spectroscopy (FTIR). The intrinsic moisture permeation barrier properties were investigated by means of the Ca test. Furthermore, their microstructure, in terms of residual open nanoporosity content, was investigated by means of ellipsometric porosimetry (EP).

In this work, in parallel with our very recent work reported for oxide barrier layers,[28,29,35] we investigated the correlation between the relative content of open porosity in SiN_x layers and their intrinsic moisture permeation barrier properties. We show that, irrespective of the deposition temperature and hence impurity content in the SiN_x films, no open pores larger than 0.3 nm in diameter are present. This leads to SiN_x barrier layers exhibiting a WVTR of 10^{-6} g/m^2/day, which is competitive with that of state-of-the-art PECVD SiN_x. Furthermore, the achieved results actually go beyond the state of the art when we consider that the same water barrier performance is achieved for an ALD film thickness of only 10 nm (vs a few hundred nanometers thick PECVD SiN_x).

2. EXPERIMENTAL SECTION

2.1. ALD of SiN_x. The ALD SiN_x depositions were carried out, as previously reported by our group,[33,34] using an Oxford Instruments FlexAL reactor, described in detail elsewhere.[41] $SiH_2(NH^tBu)_2$ (BTBAS, purity ≥98.5%, Air Products Inc.) was used as the precursor and held at a bubbler temperature of 50 °C. The precursor was introduced vapor drawn, with Ar (25 sccm, purity 99.999%) used as the carrier gas. The Ar was also used for purging. The delivery lines were heated at 70 °C to prevent condensation. The reactor was equipped with a remote inductively coupled (ICP) plasma generator, which was operated at 600 W at 13.56 MHz. A mixture of N_2 (100 sccm, purity 99.999%) and Ar (200 sccm) was used to generate the plasma. The wall temperature was set equal to the deposition temperature, with a maximum of 150 °C. A base pressure in the reactor chamber of ~10^{-6} Torr was reached by a turbo-pump. The operating pressure was controlled by setting a butterfly valve at 10° during precursor dosing and reacting (80 mTorr) and at 90° during the plasma exposure and purging for maximal pumping (24 mTorr).

For analysis of the material's properties, films were deposited on *c*-Si substrates with a thin native oxide (SiO_2) layer. No additional cleaning steps were undertaken. 100 nm thick SiN_x layers were deposited at 80, 120, 160, and 200 °C. The substrates were heated for 30 min prior to deposition. The optimized ALD process cycle is schematically depicted in Figure 1.

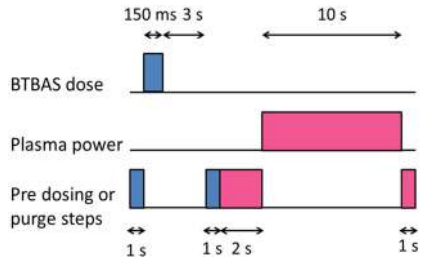

Figure 1. Schematic of the ALD process cycle, consisting of the following steps: predosing purge of the delivery line (1 s), precursor dosing (150 ms), reaction step (3 s), precursor purge (1 s), predosing purge of the plasma source (2 s), plasma exposure (10 s), and plasma purge step (1 s).

2.2. SiN_x Material Analysis. The film thickness and optical properties of the layers were measured by spectroscopic ellipsometry, using a J.A. Woollam Co. M-2000F ellipsometer and collecting data over a wavelength range of 400−1000 nm. The measurements were performed in vacuum at an incidence angle of 70° and analyzed using J.A. Woollam Complete EASE software, version 4.91. The optical model used consists of a silicon substrate, 1.5 nm native oxide, and a silicon nitride layer modeled with a Cauchy dispersion relation, without taking surface roughness into account (AFM surface roughness measurements indicate a low RMS roughness of 0.3 ±

DOI: 10.1021/acsami.5b06801
ACS Appl. Mater. Interfaces 2015, 7, 22525−22532

Table 1. Growth per Cycle (GPC), Refractive Index, and Atomic Composition of 100 nm Thick SiN_x Films Prepared at Different Deposition Temperatures on Native Oxide Covered *c*-Si Substrates[a]

			XPS			ERD
temp. (°C)	GPC (nm/cycle)	n_{633nm}	N/Si	[C] (atom %)	[O] (atom %)	[H] (atom %)
80	0.044 ± 0.002	1.802 ± 0.005	1.9 ± 0.1	14 ± 1	2 ± 1	12 ± 1
120	0.033	1.839	1.7	9	3	11
160	0.026	1.884	1.6	6	3	n.d.
200	0.024	1.904	1.6	5	2	8

[a]The typical error bars are indicated in the first row.

0.1 nm). The chemical composition and stoichiometry of the SiN_x films were investigated with X-ray photoelectron spectroscopy (XPS), using a Thermo Scientific K-Alpha spectrometer with a monochromatic Al Kα X-ray source ($h\nu$ = 1486.6 eV). Depth profiles were measured through sputtering with Ar^+ ions. Further chemical characterization of the SiN_x films was carried out by means of Fourier-transform infrared spectroscopy (FTIR) with a Bruker Tensor 27 spectrophotometer. The spectrometer was purged with N_2 prior to spectra acquisition. The FTIR spectra were recorded in transmission mode in the range 400−4000 cm^{-1} with a resolution of 4 cm^{-1}. The reported FTIR spectra are baseline corrected and normalized with respect to the layer thickness. All characterization was performed either directly after deposition or after storage of the films in a glovebox, to prevent aging of the SiN_x layers.

2.3. Ellipsometric Porosimetry Measurements. The porosity of the 100 nm thick SiN_x films deposited on the *c*-Si substrates at 80, 120, 160, and 200 °C was investigated with ellipsometric porosimetry. Ellipsometric porosimetry provides information on the open porosity and pore size distribution present in the layers.[36−40] The quantification of the porosity strongly depends on the size of the probe molecules. Here, multisolvent EP measurements were performed using water, ethanol, and toluene. These solvents are volatile liquids that can be employed at room temperature and differ in kinetic diameter and polarity. EP relies on the change of the optical properties of the film during vapor adsorption and desorption. The adsorption of probe molecules leads to a variation of the refractive index (n) and the development of an adsorbate multilayer, which are both monitored by SE. Classical adsorption/desorption isotherms can be obtained by plotting the variation of the optical properties as a function of the relative pressure, defined as the ratio between the equilibrium partial pressure (P_l) and the vapor pressure (P_{sat}) of the probing liquid.

An in-house built porosimeter was used, based on a setup extensively described in refs 29, 37, and 39. The porosimeter consisted of a vacuum chamber, equipped with a spectroscopic ellipsometer, a turbo- and backing pump, Ar carrier gas, and an adsorptive line.[28] Three solvents were adopted: water (kinetic diameter ∼ 0.3 nm, P_{sat} ∼ 31.6 mbar at 25 °C), ethanol (∼0.4 nm, P_{sat} ∼ 78.3 mbar at 25 °C), and toluene (∼0.6 nm, P_{sat} ∼ 37.9 mbar at 25 °C). The polarity values of the solvents are 80 for water (polar), 24.6 for ethanol (polar), and 2.4 for toluene (nonpolar). The stainless steel tubings and chamber were heated at 50 °C to prevent condensation of the adsorptive on the walls, and the substrate table was kept at 25 °C by a built-in Peltier heater.

Before starting the measurement, the SiN_x films were allowed to outgas overnight in the porosimeter in vacuum (10^{-5} mbar) at 25 °C. During the adsorption and desorption sequence, the P_l/P_{sat} set point was increased step-by-step from 0 to 1 and then decreased again. In order to cover the full P_l/P_{sat} range, several set points for the pressure in the porosimeter and for the total flow rate were used. The pressure was set at 150, 500, or 900 mbar, and the total flow rate was varied between 750 and 2500 mg/min. The required liquid and gas flow rates were then automatically calculated and adapted to deliver vapor with the desired P_l/P_{sat}. A step duration of 10 min was chosen for each step in vapor pressure to provide adsorption−desorption equilibrium between the adsorbed phase and the gas phase. The optical properties were continuously monitored using the same type of ellipsometer and settings as described in Section 2.2. The refractive index of the SiN_x and the adsorptive layer thickness were determined for each value of vapor pressure by taking an average of the data recorded after the equilibrium has been reached (last 4 min of each step). The SE data was modeled in the 400−1000 nm range with a model consisting of a silicon substrate, ∼1.5 nm SiO_2 native oxide, a Cauchy function for SiN_x, and an additional layer for the adsorptive multilayer thickness. In this fitting procedure, the simplest physical model has been chosen with the fewest number of fitting parameters. Alternative and more complex models, such as the Tauc−Lorentz model, which is more commonly used to describe SiN_x, have been found not to improve the robustness and fit uniqueness. The Cauchy function is shown in eq 1

$$n(\lambda) = A + \frac{B}{\lambda^2} + \frac{C}{\lambda^4} \quad (1)$$

where λ is the wavelength and A, B, and C are the Cauchy fitting parameters. The SiN_x layer was fitted when P_l/P_{sat} = 0 using A, B, k, and the thickness (d) as fitting parameters. The obtained k (<0.005) and d_{SiN_x} (∼100 nm) were kept constant (i.e., no swelling of the layer was observed) during the adsorption/desorption measurements, whereas the adsorptive multilayer thickness $d_{adsorptive}$ and A and B for the SiN_x layer were fitted to obtain the adsorptive multilayer thickness and the refractive index of the SiN_x layer during the porosimetry analysis. The adsorbed water layer was modeled as described in ref 42 (n_{H_2O} = 1.331 at λ = 632.8 nm). A Cauchy layer was applied to model the ethanol[43] ($n_{C_2H_5OH}$ = 1.360) and toluene[44] ($n_{C_6H_5CH_3}$ = 1.486) layers using fixed A, B, and C values and d as a fitting parameter.

2.4. Evaluation of Barrier Performance. The intrinsic barrier performance of the SiN_x thin films has been evaluated by means of the calcium test.[2,45] The followed procedure and setup are described in detail in refs 10, 29, and 30. Briefly, 40 nm Ca was thermally evaporated on 150 × 150 mm^2 glass plates in a pattern of nine pads each consisting of nine squares. On top of the Ca, 40 nm SiO_2 with a WVTR of 10^{-2} g/m^2/day was deposited by PE-CVD in order to serve as temporary barrier against moisture permeation during sample transport. Finally, 10, 20, and 40 nm thick SiN_x barriers were deposited by ALD at 120 °C. This low deposition temperature ensures compatibility of the barrier deposition process with organic semiconductors and polymer substrates. The test plates were then placed in an environmental chamber at 20 °C and 50% relative humidity. Pictures of the samples were taken periodically, and the amount of oxidation was determined from the gray scale image. Ideally, the WVTR is calculated when at least 1 nm of the Ca material has been oxidized.[10] In the Ca test samples, however, a large number of pinholes was present due to particle formation during Ca deposition. Because of permeation through defects in the barrier, white spots occurred that covered, in the majority of pads, the entire Ca pad before 1 nm Ca had been oxidized uniformly. Areas containing white spots were excluded, therefore, and the WVTR was averaged over the remaining areas. The detection limit of the intrinsic WVTR is on the order of 10^{-6} g/m^2/day.

3. RESULTS AND DISCUSSION

3.1. SiN_x Optical and Chemical Characterization. The SiN_x growth per cycle (GPC), thin-film refractive index (n),

DOI: 10.1021/acsami.5b06801
ACS Appl. Mater. Interfaces 2015, 7, 22525−22532

and chemical composition in the bulk of the layer are reported in Table 1 for the indicated T_{sub}. The GPC decreases with increasing deposition temperature. The lower GPC at higher deposition temperature is a result of the lower impurity content (e.g., carbon) due to more efficient ligand abstraction at higher temperature, resulting in higher film density. This conclusion is supported by the trends in refractive index and chemical composition. The refractive index ranges from approximately 1.80 for SiN_x deposited at 80 °C to 1.90 for that at 200 °C. The N/Si ratio, as determined by XPS, is higher than the stoichiometric ratio, but it approaches the latter value when the deposition temperature increases. Depth profile XPS measurements show that the C impurity levels range from 14 atom % for SiN_x deposited at 80 °C to 5 atom % for SiN_x deposited at 200 °C, confirming that more efficient ligand abstraction takes place at higher temperatures. The O content is constant at 2−3% and is related to the presence of residual O_2 or moisture in the process chamber during deposition. The H content has been determined previously for SiN_x layers deposited with the same process using slightly different process conditions.[33] By comparing the present refractive index and carbon contamination level with previously measured values, it can be inferred that the H level is between 12 ± 1 atom % for SiN_x deposited at 80 °C and 8 ± 1 atom % for SiN_x deposited at 200 °C. Comparable values have been obtained for SiN_x layers deposited by a monomer very similar to BTBAS, namely, di(*sec*-butyl)aminosilane (DSBAS), processed under the same conditions as reported in this article. The layers deposited at 100 °C have the same refractive index and carbon and oxygen contamination levels as those found in the layers deposited from the BTBAS process at 120 °C, and they are characterized by a H concentration of 11 ± 1%. In addition, at 200 °C, the DSBAS process is characterized by the same H content of 8 ± 1% (and N/Si ratio and impurity levels) as that of the BTBAS process.

The chemical composition of the SiN_x layers deposited at the indicated T_{sub} was also investigated with FTIR. Typical FTIR spectra are shown in Figure 2. The characteristic (hydrogenated) SiN_x absorption peaks visible in the spectra are the N−H stretching mode at ∼3345 cm^{-1}, the Si−H stretching mode at ∼2180 cm^{-1} for different back bondings, the N−H rocking mode at ∼1195 cm^{-1}, the Si−N−Si asymmetric stretching mode at ∼895 cm^{-1}, and the Si−N bending mode at 470 cm^{-1}.[30,46,47] The FTIR spectra confirm the presence of oxygen and carbon. An absorption peak at ∼1105 cm^{-1} of the Si−O−Si asymmetric stretching mode, a peak at ∼795 cm^{-1} of the symmetric stretching mode, and a small peak at 515 cm^{-1} of the Si−O bending mode in the spectrum of the 80 °C SiN_x indicate the presence of oxygen in the layer.[48] The absorption peak around 3300−3700 cm^{-1}, typical for Si−OH, is not detected. The absorption at 582 cm^{-1} is tentatively attributed to Si−C bonds.[49] This is confirmed by the deconvolution of the C 1s peak measured by XPS that shows a component at a binding energy of 283.7−284.1 eV, indicating Si−C bonds. Another impurity peak observed around 1600 cm^{-1} is attributed to the C═O stretching mode in amides and/or the N−H bending mode in amines. The carbonyl functionality can occur because of the partial oxidation process of residual *t*-butyl groups during the plasma exposure step due to the presence of residual O_2 or H_2O in the chamber. The absence of C−H stretching peaks between 2800 and 3000 cm^{-1} indicates that there is not a significant amount of organic (unoxidized) species present in the layer.

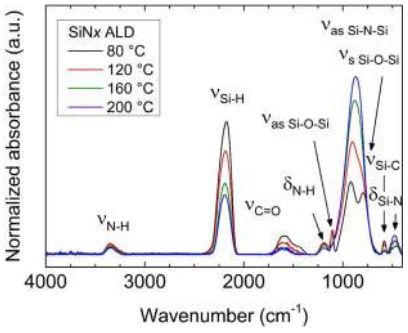

Figure 2. Fourier-transform infrared spectroscopy (FTIR) data of the SiN_x films deposited at the indicated substrate temperatures. The spectra were normalized with respect to the layer thickness, which was measured to be approximately 100 nm. Stretching (ν) and bending (δ) modes are indicated.

For increasing deposition temperatures, a shift of the peak positions of the Si−H and Si−N−Si absorption bands is observed. The peak position of the Si−H stretching mode shifts from 2190 cm^{-1} for 80 °C toward lower wavenumber values as the temperature increases, i.e., 2175 cm^{-1} for 200 °C. Similarly, the Si−N−Si asymmetric stretching mode is found at 920 cm^{-1} for 80 °C, and it shifts toward 870 cm^{-1} for 200 °C. The shift toward lower wavenumbers points out the less electronegative environment of Si at higher deposition temperatures. The level of impurities is indeed clearly dependent on the deposition temperature. The Si−N−Si stretching vibration peaks become stronger with increasing deposition temperature, and at the same time, all C, O, and H contamination-related absorption bands decrease in intensity. The reduction of the contamination levels for higher deposition temperatures is consistent with the XPS data.

The incorporation of C, O, and H impurities in the ALD SiN_x layers is in line with observations by Gumpher et al. for the LPCVD of SiN_x with BTBAS as a precursor.[49] The incorporation of these impurities results in a lower density and a lower refractive index as compared to those of vitreous, stoichiometric Si_3N_4 (2.01[50]). Since the refractive index of thermal silica (1.465) is lower than that of *a*-SiN_x:H, the incorporation of oxygen also reduces the refractive index of *a*-SiN_x:H. Furthermore, previous studies have established a correlation between the H content and the refractive index, where a higher H content correlates with a decrease in the refractive index.[51]

3.2. Open Porosity Evaluation in SiN_x Layers. Figure 3 shows the adsorption/desorption isotherms for the 100 nm thick SiN_x layers deposited at 80, 120, 160, and 200 °C when water, ethanol, and toluene are adopted as adsorptives. The change in the optical thickness of the SiN_x layer combined with the optical thickness of the adsorptive layer, presented in eq 2, has been reported as a function of P_l/P_{sat}. The change in optical thickness accounts for the total adsorbed quantity of the probe molecule.

$$\Delta \text{ optical thickness} = n_{SiN_x} \times d_{SiN_x} + n_{solvent} \times d_{multilayer} - n_{SiN_x,vacuum} \times d_{SiN_x,vacuum} \quad (2)$$

The shapes of the adsorption curves are characterized by a type II isotherm associated with nonporous layers, according to the IUPAC classification[52] (see inset in Figure 5b). The observed

DOI: 10.1021/acsami.5b06801
ACS Appl. Mater. Interfaces 2015, 7, 22525−22532

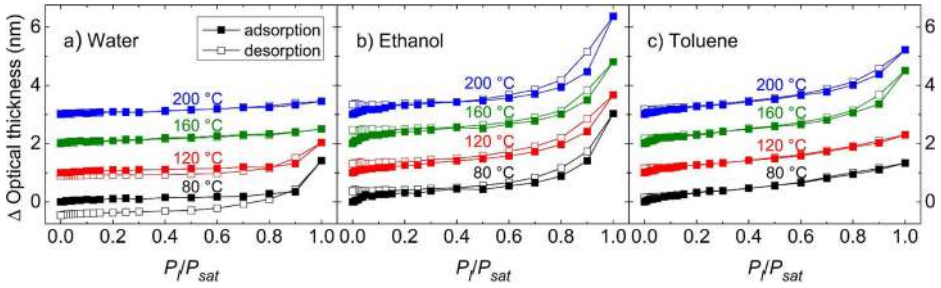

Figure 3. Adsorption/desorption isotherms obtained with multisolvent ellipsometric porosimetry for SiN_x layers prepared at various temperatures. The change in optical thickness (at 633 nm) of the SiN_x and the adsorptive multilayer is presented as a function of relative vapor pressure (P_l/P_{sat}) for (a) water, (b) ethanol, and (c) toluene. The isotherms are vertically offset by 1, 2, and 3 nm for clarity. The experimental error of the change is optical thickness is ±0.1 nm.

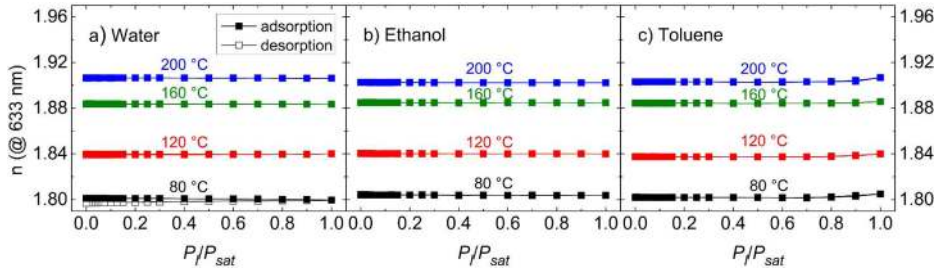

Figure 4. Refractive index as a function of P_l/P_{sat} during adsorption and desorption of water (a), ethanol (b), and toluene (c) on SiN_x samples prepared at various temperatures. The experimental error of n is ±0.005.

small increase at $P_l/P_{sat} < 0.2$ is attributed to the adsorptive monolayer formation, followed by multilayer formation that further develops as P_l/P_{sat} approaches 1. This unrestricted multilayer growth is typical for nonporous layers. For all three solvents, a steep increase of the optical thickness in the $P_l/P_{sat} < 0.2$ range, typical for micropore filling,[29] is not observed.

To better discern between the two contributions to the optical thickness, the refractive index of the SiN_x layer and adsorptive layer thickness are separately presented in Figures 4 and 5, respectively. The refractive index of the SiN_x layers remains constant upon increasing the vapor pressure for all solvents, indicating that no infiltration of the probing molecules in the SiN_x layer occurs. Taking into account the size of the smallest probe molecule, i.e., water, it can be concluded that no nanopores larger than 0.3 nm are present in the films. Even though the layers exhibit different refractive indices that are dependent on the SiN_x deposition temperature, and the FTIR and XPS analyses clearly demonstrate that the impurity levels increase when lowering the deposition temperature, it can be concluded from the EP analysis that open porosity is absent in all investigated layers.

A very limited clockwise hysteresis is observed in the water EP measurement for the samples deposited at 80 and 120 °C (see Figures 3a and 4a). The decrease of n for 80 °C after adsorption and desorption is only around 0.004. Note that the direction is different from the more common anticlockwise hysteresis caused by trapping of the probe molecules in the pores.[38,39] The decrease of the refractive index may be attributed to oxidation possibly by oxygen, which becomes more pronounced for films with higher C content, which are obtained at the lowest temperatures.[33]

The main effect of increasing P_l/P_{sat} is an increase in multilayer thickness of the probe molecule on top of the nonporous barrier layer. The thickness of the solvent layer adsorbed on the SiN_x is presented in Figure 5 as a function of the relative pressure. The shapes of the thickness adsorption isotherms are obviously similar to the overall adsorption isotherm, described by type II behavior (depicted in the inset of Figure 5b). At low relative pressure, the shape of the curves is convex and an inflection point can be observed, indicative of the completion of a monolayer and the beginning of multilayer uptake. The thickness of the multilayer at the saturation pressure depends on the SiN_x deposition temperature and the polarity of the solvent used. The multilayer thickness of water decreases with deposition temperature, whereas, on the other hand, the multilayer thickness of nonpolar toluene increases with deposition temperature. The multilayer thickness observed with ethanol, which has a polarity in between that of water and toluene, decreases slightly with deposition temperature. The SiN_x layer is hydrophilic, and a lower deposition temperature leads to layers with more impurities and therefore a higher polarity. The higher polarity of these layers promotes the interaction with polar solvents and suppresses the adsorption of nonpolar solvents, which is in line with the trends observed. Irrespective of the impurity content of the tested SiN_x films, the multilayer formation follows a type II isotherm, and no uptake of solvent in the barriers is present. These results confirm the nonporous nature of the SiN_x films.

3.3. Ca Test and WVTR Measurements. EP measurements on the ALD SiN_x layers showed that no nanopores larger than 0.3 nm are present for each deposition temperature. Previously, it has been demonstrated for oxides that the absence of porosity larger than 0.3 nm leads to an excellent moisture barrier with a WVTR in the range of 10^{-6} g/m^2/day.[28,29] Therefore, we tested the intrinsic barrier properties of the SiN_x layers deposited at only 120 °C with the Ca test. Figure 6 shows an example of a Ca plate encapsulated with 40 nm of SiN_x at the start of the Ca test and after 53 and 109 days of testing. The uniform change in grayscale due to the oxidation of Ca over time, which determines the intrinsic WVTR of the

DOI: 10.1021/acsami.5b06801
ACS Appl. Mater. Interfaces 2015, 7, 22525−22532

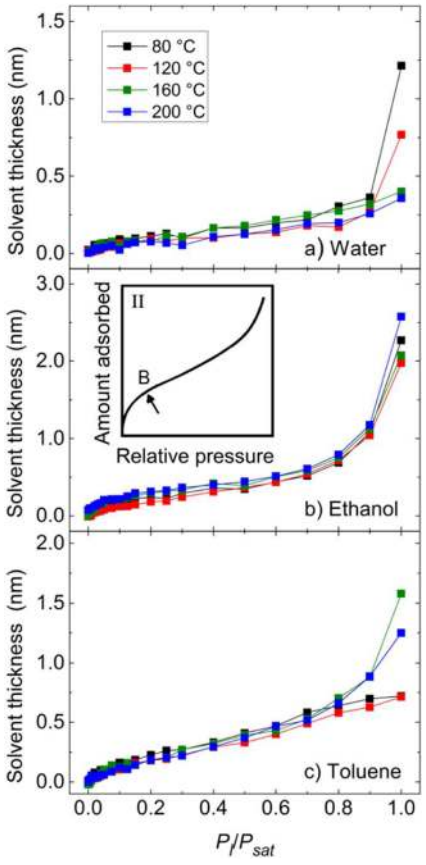

Figure 5. Adsorptive layer thickness development as a function of P_l/P_{sat} during adsorption of water (a), ethanol (b), and toluene (c) on SiN_x samples deposited at the indicated temperatures. In the inset of (b), a nonporous (type II) adsorption/desorption isotherm is shown, according to the IUPAC classification. The inflection point, B, is related to the completion of the first adsorbed monolayer and the beginning of multilayer adsorption. The experimental error of the solvent thickness is ±0.1 nm.

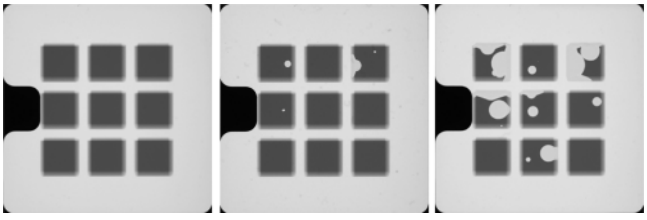

Figure 6. Optical images of a calcium test plate protected with 40 nm of ALD SiN_x at 0, 53, and 109 days of testing at 20 °C and 50% RH. The grayscale of the 5 × 5 mm^2 Ca squares is periodically monitored to estimate the intrinsic WVTR. The white spots on the calcium squares are due to local water vapor permeation through defects in the encapsulation layer.

barrier, is not visible to the naked eye. The effect of pinholes, however, is clearly visible as white spots that develop in size and density. In many of the Ca test samples, a large number of pinholes is present due to particles on the Ca test plates. Because of the high conformality, ALD can cover most pinholes and particles, but due to stress around the covered defects, the covered pinholes can be easily damaged during handling. The area of the interdefect regions necessary for determining the intrinsic WVTR decreased over time, thereby reducing the available data points in the Ca test.

The intrinsic WVTR values of the SiN_x barrier films are shown in Figure 7 for the 10, 20, and 40 nm layers. After 109

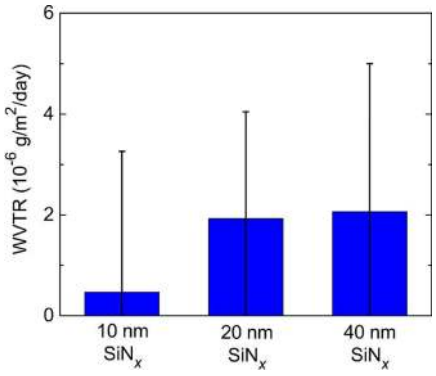

Figure 7. Intrinsic water vapor transmission rates (WVTR) measured for 10, 20, and 40 nm SiN_x films prepared by ALD at 120 °C. Data is shown for after 2600 h in 20 °C and 50% relative humidity.

days, only ~0.35 nm of Ca has been oxidized. To obtain results with 10% precision, the test should last until at least 1 nm of the Ca material has been oxidized; therefore, the error margin is large. The SiN_x layers have an intrinsic WVTR on the order of 10^{-6} g/m^2/day, which is required for OLED encapsulation. The same barrier performance is expected for the SiN_x layers deposited at 80 °C because ellipsometric porosimetry measurements show no microporosity for these layers. Strikingly, the measured intrinsic WVTR is, within the error margin, not dependent on the SiN_x layer's thickness. Apparently, just a 10 nm thick ALD SiN_x is sufficient to guarantee the formation of a continuous layer. The ALD SiN_x barriers combine the benefits of SiN_x as a material with high conformality and high density typical of ALD layers. The obtained intrinsic WVTR values of the ultrathin ALD SiN_x barriers compare with the best intrinsic WVTR values reported in literature.

4. CONCLUSIONS

Thin films of SiN_x deposited by low-temperature plasma-assisted atomic layer deposition have been investigated for application as moisture permeation barriers. The films deposited at 80−200 °C have been characterized in terms of their refractive index and chemical composition by SE, XPS, and FTIR. The SiN_x thin-film refractive index ranges from 1.80 when deposited at 80 °C to 1.90 when deposited at 200 °C, and the C and O levels decrease when the deposition temperature increases, down to 5 atom % C and 2 atom % O for 200 °C.

The microstructure of the layers has been studied by ellipsometric porosimetry, using water, ethanol, and toluene as probe molecules. The adsorption isotherms are, according to the IUPAC classification, characterized by a type II (nonporous) shape for all solvents. The refractive index of the SiN_x layers remains constant upon increasing the adsorptive vapor pressure, indicating that there is no infiltration of the probing molecules into the nonporous SiN_x layer for all adsorptives and deposition temperatures. The main effect of increasing P_l/P_{sat} is the development of a multilayer of the probe molecule on top of the nonporous barrier layer. These results demonstrate the nonporous nature of the SiN_x films and are in good agreement with the excellent intrinsic WVTR values obtained. The intrinsic moisture barrier properties of SiN_x barriers deposited at 120 °C evaluated with the calcium test reveal excellent

DOI: 10.1021/acsami.5b06801
ACS Appl. Mater. Interfaces 2015, 7, 22525−22532

barrier properties in the range of 10^{-6} g/m^2/day for SiN_x layers as thin as 10 nm.

AUTHOR INFORMATION

Corresponding Author

*E-mail: m.creatore@tue.nl. Phone: +31 402474223.

Notes

The authors declare no competing financial interest.

ACKNOWLEDGMENTS

The authors would like to thank Pieter Klaassen and Marc Kuilder (Philips Research, High Tech Campus, Eindhoven, The Netherlands) and Jie Shen and Dr. Jasper Michels (Holst Centre, High Tech Campus, Eindhoven, The Netherlands) for the Ca tests as well as Dr. Valerio Zardetto for the XPS measurements. Wytze Keuning, Cristian van Helvoirt, Paul Aendenroomer, Ries van de Sande, Joris Meulendijks, and Janneke Zeebregts are thanked for their excellent technical assistance. This work was financially supported by Nano-NextNL, a micro- and nanotechnology programme of the Dutch Ministry of Economic Affairs, Agriculture and Innovation (EL&I) and 130 partners. M.C. and A.P. acknowledge the Aspasia-NWO program and Dutch Polymer Institute (DPI) project no. 752 of the Large Area Thin Film Electronics (LATFE) program, respectively.

REFERENCES

(1) Forrest, S. The Path to Ubiquitous and Low-Cost Organic Electronic Appliances on Plastic. *Nature* **2004**, *428*, 911−918.

(2) van de Weijer, P.; van Mol, A. M. B. *White Paper on the Characterisation of Thin-Film Barrier Layers for Protection of Organic Light-Emitting Diodes*, Project ICT-216641, Fast2Light, 2009

(3) Park, J.-S.; Chae, H.; Chung, H.; Lee, S. Thin Film Encapsulation for Flexible AM-OLED: A Review. *Semicond. Sci. Technol.* **2011**, *26*, 034001.

(4) Feron, K.; Nagle, T.; Rozanski, L.; Gong, B.; Fell, C. Spatially Resolved Photocurrent Measurements of Organic Solar Cells: Tracking Water Ingress at Edges and Pinholes. *Sol. Energy Mater. Sol. Cells* **2013**, *109*, 169−177.

(5) Dennler, G.; Lungenschmied, C.; Neugebauer, H.; Sariciftci, N.; Latrèche, M.; Czeremuszkin, G.; Wertheimer, M. A New Encapsulation Solution for Flexible Organic Solar Cells. *Thin Solid Films* **2006**, *511−512*, 349−353.

(6) Lin, H.; Xu, L.; Chen, X.; Wang, X.; Sheng, M.; Stubhan, F.; Merkel, K.-H.; Wilde, J. Moisture-Resistant Properties of SiN_x Films Prepared by PECVD. *Thin Solid Films* **1998**, *333*, 71−76.

(7) Vogt, M.; Hauptmann, R. Plasma-Deposited Passivation Layers for Moisture and Water Protection. *Surf. Coat. Technol.* **1995**, *74−75*, 676−681.

(8) Huang, W.; Wang, X.; Sheng, M.; Xu, L.; Stubhan, F.; Luo, L.; Feng, T.; Wang, X.; Zhang, F.; Zou, S. Low Temperature PECVD SiN_x Films Applied in OLED Packaging. *Mater. Sci. Eng., B* **2003**, *98*, 248−254.

(9) Lievens, H. Wide Web Coating of Complex Materials. *Surf. Coat. Technol.* **1995**, *76−77*, 744−753.

(10) Keuning, W.; van de Weijer, P.; Lifka, H.; Kessels, W.; Creatore, M. Cathode Encapsulation of Organic Light Emitting Diodes by Atomic Layer Deposited Al_2O_3 Films and Al_2O_3/a-SiN_x:H Stacks. *J. Vac. Sci. Technol., A* **2012**, *30*, 01A131.

(11) Carcia, P.; McLean, R.; Reilly, M.; Groner, M.; George, S. Ca Test of Al_2O_3 Gas Diffusion Barriers Grown by Atomic Layer Deposition on Polymers. *Appl. Phys. Lett.* **2006**, *89*, 031915.

(12) Yong-Qiang, Y.; Yu, D.; Ya-Hui, D.; Xiao, W.; Ping, C.; Dan, Y.; Feng-Bo, S.; Kai-wen, X. High Barrier Properties of Transparent Thin-Film Encapsulations for Top Emission Organic Light-Emitting Diodes. *Org. Electron.* **2014**, *15*, 1120−1125.

(13) Jung, H.; Jeon, H.; Choi, H.; Ham, G.; Shin, S.; Jeon, H. Al_2O_3 Multi-Density Layer Structure as a Moisture Permeation Barrier Deposited by Radio Frequency Remote Plasma Atomic Layer Deposition. *J. Appl. Phys.* **2014**, *115*, 073502.

(14) Seo, S.-W.; Jung, E.; Lim, C.; Chae, H.; Cho, S. Moisture Permeation through Ultrathin TiO_2 Films Grown by Atomic Layer Deposition. *Appl. Phys. Express* **2012**, *5*, 035701.

(15) Duan, Y.; Sun, F.; Yang, Y.; Chen, P.; Yang, D.; Duan, Y.; Wang, X. Thin-Film Barrier Performance of Zirconium Oxide Using the Low-Temperature Atomic Layer Deposition Method. *ACS Appl. Mater. Interfaces* **2014**, *6*, 3799−3804.

(16) Meyer, J.; Schneidenbach, D.; Winkler, T.; Hamwi, S.; Weimann, T.; Hinze, P.; Ammermann, S.; Johannes, H.; Riedl, T.; Kowalsky, W. Reliable Thin Film Encapsulation for Organic Light Emitting Diodes Grown by Low-Temperature Atomic Layer Deposition. *Appl. Phys. Lett.* **2009**, *94*, 233305.

(17) Carcia, P.; McLean, R.; Groner, M.; Dameron, A.; George, S. Gas Diffusion Ultrabarriers on Polymer Substrates Using Al_2O_3 Atomic Layer Deposition and SiN Plasma-Enhanced Chemical Vapor Deposition. *J. Appl. Phys.* **2009**, *106*, 023533.

(18) Langereis, E.; Creatore, M.; Heil, S.; van de Sanden, M. C. M.; Kessels, W. Plasma-Assisted Atomic Layer Deposition of Al_2O_3 Moisture Permeation Barriers on Polymers. *Appl. Phys. Lett.* **2006**, *89*, 081915.

(19) Kim, N.; Graham, S. Development of Highly Flexible and Ultra-Low Permeation Rate Thin-Film Barrier Structure for Organic Electronics. *Thin Solid Films* **2013**, *547*, 57−62.

(20) da Silva Sobrinho, A. S.; Czeremuszkin, G.; Latrèche, M.; Wertheimer, M. R. Defect-Permeation correlation for ultrathin transparent barrier coatings on polymers. *J. Vac. Sci. Technol., A* **2000**, *18* (1), 149−157.

(21) Erlat, A. G.; Wang, B.-C.; Spontak, R. J.; Tropsha, Y.; Mar, K. D.; Montgomery, D. B.; Vogler, E. A. Morphology and Gas Barrier Properties of Thin SiO_x Coatings on Polycarbonate: Correlations with Plasma-Enhanced Chemical Vapor Deposition Conditions. *J. Mater. Res.* **2000**, *15*, 704−717.

(22) Burrows, P.; Graff, G.; Gross, M.; Martin, P.; Shi, M.; Hall, M.; Mast, E.; Bonham, C.; Bennett, W.; Sullivan, M. Ultra Barrier Flexible Substrates for Flat Panel Displays. *Displays* **2001**, *22*, 65−69.

(23) Graff, G.; Williford, R.; Burrows, P. Mechanisms of Vapor Permeation through Multilayer Barrier Films: Lag Time versus Equilibrium Permeation. *J. Appl. Phys.* **2004**, *96*, 1840−1849.

(24) Weaver, M.; Michalski, L.; Rajan, K.; Rothman, M.; Silvernail, J.; Brown, J.; Burrows, P.; Graff, G.; Gross, M.; Martin, P.; et al. Organic Light-Emitting Devices with Extended Operating Lifetimes on Plastic Substrates. *Appl. Phys. Lett.* **2002**, *81*, 2929−2931.

(25) Chen, T.; Wuu, D.; Wu, C.; Chiang, C.; Chen, Y.; Horng, R. High-Performance Transparent Barrier Films of SiO_x/SiN_x Stacks on Flexible Polymer Substrates. *J. Electrochem. Soc.* **2006**, *153*, F244.

(26) Roberts, A.; Henry, B.; Sutton, A.; Grovenor, C.; Briggs, G.; Miyamoto, T.; Kano, M.; Tsukahara, Y.; Yanaka, M. Gas Permeation in Silicon-Oxide/Polymer (SiO_x/PET) Barrier Films: Role of the Oxide Lattice, Nano-Defects and Macro-Defects. *J. Membr. Sci.* **2002**, *208*, 75−88.

(27) Affinito, J.; Hilliard, D. *A New Class of Ultra-Barrier Materials*, Society of Vacuum Coaters, 47th Annual Technical Conference Proceedings, Dallas TX, April 24−29, 2004; pp 563−593.

(28) Perrotta, A.; Garcia, S. J.; Creatore, M. Ellipsometric Porosimetry and Electrochemical Impedance Spectroscopy Characterization for Moisture Permeation Barrier Layers. *Plasma Processes Polym.* **2015**, *12*, 968.

(29) Perrotta, A.; Van Beekum, E. R. J.; Aresta, G.; Jagia, A.; Keuning, W.; van de Sanden, R. M. C. M.; Kessels, E.; Creatore, M. On the Role of Nanoporosity in Controlling the Performance of Moisture Permeation Barrier Layers. *Microporous Mesoporous Mater.* **2014**, *188*, 163−171.

(30) van Assche, F.; Unnikrishnan, S.; Michels, J.; van Mol, A. M. B.; van de Weijer, P.; van de Sanden, M. C. M.; Creatore, M. On the

DOI: 10.1021/acsami.5b06801
ACS Appl. Mater. Interfaces 2015, 7, 22525−22532

Intrinsic Moisture Permeation Rate of Remote Microwave Plasma-Deposited Silicon Nitride Layers. *Thin Solid Films* **2014**, *558*, 54−61.
(31) Koehler, F.; Triyoso, D.; Hussain, I.; Mutas, S.; Bernhardt, H. Atomic Layer Deposition of SiN for Spacer Applications in High-End Logic Devices. *IOP Conf. Ser.: Mater. Sci. Eng.* **2012**, *41*, 012006.
(32) Murray, C.; Elliott, S.; Hausmann, D.; Henri, J.; LaVoie, A. Effect of Reaction Mechanism on Precursor Exposure Time in Atomic Layer Deposition of Silicon Oxide and Silicon Nitride. *ACS Appl. Mater. Interfaces* **2014**, *6*, 10534−10541.
(33) Knoops, H. C. M.; Braeken, E. M. J.; de Peuter, K.; Potts, S. E.; Haukka, S.; Pore, V.; Kessels, W. M. M. Atomic Layer Deposition of Silicon Nitride from Bis(tert-butylamino)silane and N_2 Plasma. *ACS Appl. Mater. Interfaces* **2015**, *7*, 19857−19862.
(34) Knoops, H. C. M.; de Peuter, K.; Kessels, W. M. M. Redeposition in Plasma-Assisted Atomic Layer Deposition: Silicon Nitride Film Quality Ruled by the Gas Residence Time. *Appl. Phys. Lett.* **2015**, *107*, 014102.
(35) Perrotta, A.; Garcia, S. J.; Michels, J. J.; Andringa, A.-M.; Creatore, M. Analysis of Nano-Porosity in Moisture Permeation Barrier Layers by Electrochemical Impedance Spectroscopy. *ACS Appl. Mater. Interfaces* **2014**, *7*, 15968−15977.
(36) Shamiryan, D.; Baklanov, M.; Maex, K. Diffusion Barrier Integrity Evaluation by Ellipsometric Porosimetry. *J. Vac. Sci. Technol., B: Microelectron. Process. Phenom.* **2003**, *21*, 220−226.
(37) Baklanov, M.; Mogilnikov, K.; Polovinkin, V.; Dultsev, F. Determination of Pore Size Distribution in Thin Films by Ellipsometric Porosimetry. *J. Vac. Sci. Technol., B: Microelectron. Process. Phenom.* **2000**, *18*, 1385−1391.
(38) Eslava, S.; Baklanov, M.; Kirschhock, C.; Iacopi, F.; Aldea, S.; Maex, K.; Martens, J. Characterization of a Molecular Sieve Coating Using Ellipsometric Porosimetry. *Langmuir* **2007**, *23*, 12811−12816.
(39) Licitra, C.; Bouyssou, R.; Chevolleau, T.; Bertin, F. Multi-Solvent Ellipsometric Porosimetry Analysis of Plasma-Treated Porous SiOCH Films. *Thin Solid Films* **2010**, *518*, 5140−5145.
(40) Dendooven, J.; Devloo-Casier, K.; Levrau, E.; Van Hove, R.; Sree, S. P.; Baklanov, M.; Martens, J.; Detavernier, C. In Situ Monitoring of Atomic Layer Deposition in Nanoporous Thin Films Using Ellipsometric Porosimetry. *Langmuir* **2012**, *28*, 3852−3859.
(41) Heil, S.; van Hemmen, J. L.; Hodson, C.; Singh, N.; Klootwijk, J.; Roozeboom, F.; van de Sanden, M. C. M.; Kessels, W. Deposition of TiN and HfO_2 in a Commercial 200 mm Remote Plasma Atomic Layer Deposition Reactor. *J. Vac. Sci. Technol., A* **2007**, *25*, 1357−1366.
(42) Palik, E. D. *Handbook of Optical Constants of Solids II*; Academic Press: Orlanda, FL, 1991; p 1067.
(43) Rheims, J.; Köser, J.; Wriedt, T. Refractive-Index Measurements in the Near-IR Using an Abbe Refractometer. *Meas. Sci. Technol.* **1997**, *8*, 601−605.
(44) Moutzouris, K.; Papamichael, M.; Betsis, S.; Stavrakas, I.; Hloupis, G.; Triantis, D. Refractive, Dispersive and Thermo-Optic Properties of Twelve Organic Solvents in the Visible and Near-Infrared. *Appl. Phys. B: Lasers Opt.* **2014**, *116*, 617−622.
(45) Nisato, G.; Bouten, P. C. P.; Slikkerveer, P. J.; Bennett, W. D.; Graff, G. L.; Rutherford, N.; Wiese, L. Evaluating High Performance Diffusion Barriers: The Calcium Test. *Proc. Asia Display* **2001**, 1435−1438.
(46) Signore, M.; Sytchkova, A.; Dimaio, D.; Cappello, A.; Rizzo, A. Deposition of Silicon Nitride Thin Films by RF Magnetron Sputtering: A Material and Growth Process Study. *Opt. Mater.* **2012**, *34*, 632−638.
(47) Wang, X.; Huang, R.; Song, C.; Song, J.; Guo, Y. Interface Effects on the Electroluminescence Spectra in Amorphous-Si/Silicon Oxynitride Multilayer Structures. *Sci. China: Phys., Mech. Astron.* **2012**, *55*, 1194−1197.
(48) Milella, A.; Creatore, M.; Blauw, M.; van de Sanden, M. C. M. Remote Plasma Deposited Silicon Dioxide-Like Film Densification by Means of RF Substrate Biasing: Film Chemistry and Morphology. *Plasma Processes Polym.* **2007**, *4*, 621−628.
(49) Gumpher, J.; Bather, W.; Mehta, N.; Wedel, D. Characterization of Low-Temperature Silicon Nitride LPCVD from Bis(tertiary-butylamino)silane and Ammonia. *J. Electrochem. Soc.* **2004**, *151*, G353.
(50) Bååk, T. Silicon Oxynitride; a Material for GRIN Optics. *Appl. Opt.* **1982**, *21*, 1069−1072.
(51) Claassen, W.; Valkenburg, W.; Habraken, F.; Tamminga, Y. Characterization of Plasma Silicon Nitride Layers. *J. Electrochem. Soc.* **1983**, *130*, 2419−2423.
(52) Sing, K. S. W.; Everett, D. H.; Moscou, L.; Pierotti, R. A.; Rouquerol, J.; Siemieniewska, T. Reporting Physisorption Data for Gas/Solid Systems with Special Reference to the Determination of Surface Area and Porosity (Recommendations 1984). *Pure Appl. Chem.* **1985**, *57* (4), 603−619.

DOI: 10.1021/acsami.5b06801
ACS Appl. Mater. Interfaces 2015, 7, 22525−22532